

BAO+BBN revisited – Growing the Hubble tension with a 0.7km/s/Mpc constraint

N. Schöneberg,^{a,1} L. Verde,^{a,b} H. Gil-Marín,^{a,c} S. Brieden^{a,c,d}

^a*Institut de Ciències del Cosmos, Universitat de Barcelona, Martí i Franquès 1, Barcelona E08028, Spain*

^b*ICREA, Pg. Lluís Companys 23, Barcelona E08010, Spain*

^c*Institut d'Estudis Espacials de Catalunya (IEEC), Barcelona E08034, Spain*

^d*Dept. de Física Quàntica i Astrofísica, Universitat de Barcelona, Martí i Franquès 1, E-08028 Barcelona, Spain.*

E-mail: nils.science@gmail.com

ABSTRACT: The combination of Baryonic Acoustic Oscillation (BAO) data together with light element abundance measurements from Big Bang Nucleosynthesis (BBN) has been shown to constrain the cosmological expansion history to an unprecedented degree. Using the newest LUNA data and DR16 data from SDSS, the BAO+BBN probe puts tight constraints on the Hubble parameter ($H_0 = 67.6 \pm 1.0 \text{ km/s/Mpc}$), resulting in a 3.7σ tension with the local distance ladder determination from SH0ES in a Λ CDM model. In the updated BAO data the high- and low-redshift subsets are mutually in excellent agreement, and there is no longer a mild internal tension to artificially enhance the constraints. Adding the recently-developed ShapeFit analysis yields $H_0 = 68.3 \pm 0.7 \text{ km/s/Mpc}$ (3.8σ tension). For combinations with additional data sets, there is a strong synergy with the sound horizon information of the cosmic microwave background, which leads to one of the tightest constraints to date, $H_0 = 68.30 \pm 0.45 \text{ km/s/Mpc}$, in 4.2σ tension with SH0ES. The region preferred by this combination is perfectly in agreement with that preferred by ShapeFit. The addition of supernova data also yields a 4.2σ tension with SH0ES for Pantheon, and a 3.5σ tension for PantheonPLUS. Finally, we show that there is a degree of model-dependence of the BAO+BBN constraints with respect to early-time solutions of the Hubble tension, and the loss of constraining power in extended models depends on whether the model can be additionally constrained from BBN observations.

¹Corresponding author.

Contents

1	Introduction	1
2	Method and Data	3
2.1	Method	3
2.1.1	The BAO+BBN probe	3
2.1.2	Additional probes	5
2.1.3	ShapeFit	5
2.2	Data	6
3	Results	7
3.1	Impact of updated data	8
3.2	Impact of internal (in)consistencies	9
3.3	Impact of clustering information beyond BAO	10
3.4	Impact of the CMB sound horizon angle	13
3.5	Impact of Pantheon data	14
3.6	Impact of Cosmic Chronometer Data	15
3.7	The BAO+BBN probe with dark radiation	15
3.8	The BAO+BBN probe with shifted recombination	18
4	Conclusions	19
A	Supplemental data	27

1 Introduction

With current state-of-the art data, there is a significant tension within the Λ CDM model between the Hubble parameter, H_0 , as measured by the local distance ladder method from SH0ES [1] (but not limited to SH0ES, see also [2–5] for the TRGB, and [6–8] and references therein for an overview) and that indirectly inferred from the measurement of Cosmic Microwave Background (CMB) anisotropies (e.g., Planck [9] or ACT, SPT [10, 11]). This tension has been growing steadily for almost a decade [12–16] and has consequently sparked a great amount of theoretical and experimental investigations. After the uninterrupted chain of spectacular successes of the (standard) Λ CDM model over the past few decades, the high statistical significance of the tension has been interpreted as possible signature of new physics. While the theoretical side has focused on a wide variety of extensions of Λ CDM mainly influencing the CMB inference of H_0 (see [7, 17] among others), only a few models show promise. In parallel, on the experimental side a number of direct and indirect methods have been put forth to give alternative perspectives on the Hubble tension [7, 18].

Given the far-reaching implications of a claim of new physics beyond Λ CDM, it is of utmost importance to verify that the tension does not arise from a single experiment, observation or data set. The physics of the early Universe is believed to be simple and well understood and the early-Universe probe *par excellence* is the CMB: the exquisite agreement of the Λ CDM model with CMB data represent one of the major successes of the model. However CMB constraints on H_0 are indirect and thus very model-dependent.

One particularly interesting combination of probes comes from the measurements of baryonic acoustic oscillations (BAO) within tracers of the dark matter (such as luminous red galaxies (LRG), emission line galaxies (ELG), quasi-stellar objects/quasars (QSO), and the Lyman- α forest (Ly α)) combined with the determination of light element abundances that have been generated in the big bang nucleosynthesis (BBN). It is both independent of the CMB anisotropies altogether and perhaps the most tightly constraining combination of alternative data sets in terms of the Hubble tension. In particular, one working hypothesis that has gained popularity is the early-vs-late split [8, 15, 19, 20], which can now be independently cross-checked. It is particularly interesting to notice that the early time solutions favored in [21] can be further constrained independently of the CMB using the combination of BAO and BBN.

The great advantage is that it relies almost exclusively on quantities that can be determined at the background level in cosmological perturbation theory, thus being insensitive to some of the specifics of the dark matter and dark energy models. Since the BAO+BBN probes combine physics from far before (BBN) and far after (BAO) the time of recombination, they can provide an important cross-check of the assumed underlying model.

This combination is almost a decade old [22, 23] but the incredible improvement in the precision of the BAO measurements with the SDSS survey (especially DR12 in 2015) has re-sparked the interest in this combination a few years ago [24–26]. Part of this renewed interest can also be attributed to the increased statistical power of and improved internal consistency (see [26]) between Ly α - and galaxy-based BAO measurements from the recent Ly α BAO measurement performed in the context of the eBOSS survey in [25, 27] compared to their DR11 counterparts [28, 29].

As opposed to the BBN-inspired priors on the baryon density in the aforementioned analyses, in [30] an analysis has been performed with a more detailed treatment of the BBN using a variety of different BBN codes (such as [31–33]) and measurements ([34–37]). Yet, only shortly thereafter, a new measurement of the BBN-energy deuterium burning rate by the LUNA experiment [38] has allowed for increased precision of the underlying BBN codes [39, 40]. Additionally, a new release of the BAO data from DR16 [41, 42] has further decreased the uncertainties of the BAO measurements.

In this work we aim to extend the BAO+BBN analysis performed in [30] by using these current state-of-the-art data sets for both BBN and BAO, as well as furthering the investigation in several unexplored directions.

In particular, we aim to discuss if previously known internal “tensions” still persist, to add robust alternative data from the measurement of clustering, to use the tight geometrical inference of the sound horizon angle from the CMB as an external prior, to add data from supernovae or cosmic chronometers, and to check the model-dependence of this probe with particular focus on models that could hinder the underlying mechanism behind this probe.

We describe the underlying physical mechanism behind the various probes as well as the corresponding data sets employed within this work in Section 2. In Section 3 we present the results of our investigation and conclude in Section 4.

2 Method and Data

In Section 2.1 we discuss the physical observables and corresponding constrained parameters from the various cosmological probes in greater detail, largely as a review of the physical mechanisms, though formulated in a condensed way with a slightly different perspective. Still, the expert reader might want to continue directly to Section 2.2 where the data used within this work are described, or to Section 3 where the final results are shown.

2.1 Method

Here we explain the physical mechanisms behind the various measurements employed within this work with particular focus on how their combinations might create synergies.

2.1.1 The BAO+BBN probe

The combination of BAO and BBN might seem a surprising one to strongly constrain H_0 , as both probe physics from vastly different redshifts and neither of them is directly related to the Hubble parameter. However, as we will explain below, it is exactly the complementary time-scales involved that allows for a CMB-independent view of the Hubble tension that is as constraining as the local distance ladder, and almost as constraining as CMB data.

The primary component of the BAO+BBN probe is the compilation of observations of the BAO in the clustering of galaxies, quasars, or in the intergalactic medium (IGM) as probed by the Lyman- α forest. This clustering carries the imprint of a standard ruler scale, the sound horizon at radiation drag r_s . Importantly, this standard ruler is not observed directly; instead, only its angular or redshift extent can be measured, leading to constraints on the combinations of $\delta z \approx H(z)r_s$ or $\delta\theta \approx r_s/r_A$.¹ These two can be written in terms of the normalized expansion rate $E(z) = H(z)/H_0$ as $\delta z \approx (H_0 r_s)E(z)$ and $\delta\theta \approx (H_0 r_s) / \int [1/E(z)]dz$. Notice that if δz and $\delta\theta$ are measured for multiple redshifts, they can be used to disentangle the impact of the normalized expansion $E(z)$ and the product $H_0 r_s$. Since $E(z)$ contains only late-time density fractions (in flat Λ CDM it is entirely described by Ω_m) it cannot be used for direct inference of the Hubble parameter. However, the simultaneously determined product of $H_0 r_s$ would allow for a direct measurement of H_0 if there was some kind of determination of the sound horizon r_s [15, 19, 20, 43].

¹Here r_A is the usual co-moving angular diameter distance, i.e. $r_A = \int_0^z 1/H(x)dx$ in a flat Λ CDM model. For the sound horizon r_s see Equation (2.1).

This is where the importance of the BBN becomes clear, since it allows for a calibration of r_s using the measurement of the late-time normalized expansion rate. As further described in [30] the primordial abundances of light elements are very relevant both to the ratio of baryons to photons (effectively determining $\Omega_b h^2$ for a fixed² T_{CMB}) as well as the early time expansion rate (determined through any additional relativistic dark species at BBN for a fixed T_{CMB}). The former is more directly constrained through the measurement of the deuterium abundance D_H such as from [34], while the latter is more constrained through the Helium abundance Y_p (such as measured by [35–37]), though we stress that primarily their joint constraint is important (see also Fig. 1 of [30]).

The BBN inference of $\Omega_b h^2$ in this case is what allows for the calibration of the sound horizon mentioned above. In fact, the sound horizon can be written as an integral

$$r_s = \int_{z_*}^{\infty} \frac{c_s(z)}{H(z)} dz . \quad (2.1)$$

Naïvely one could imagine that here too only the product $H_0 r_s$ could be determined for a given normalized expansion rate $E(z)$, leading to a perfect degeneracy. However, in this case the *early Universe* normalized expansion rate does indirectly depend on h . This is because in Λ CDM-like and most popular extensions of this model, at high redshifts we have:

$$E(z) \approx \sqrt{\Omega_m(1+z)^3 + \omega_r/h^2(1+z)^4}, \quad (2.2)$$

where the radiation density ω_r is fixed to

$$\omega_r \approx 2.47 \cdot 10^{-5} \left[1 + \frac{7}{8} \left(\frac{4}{11} \right)^{4/3} N_{\text{eff}} \right] \left(\frac{T_{\text{cmb}}}{2.7255\text{K}} \right)^4, \quad (2.3)$$

which is measured independently of h , meaning that Equation (2.2) does depend on h . We immediately notice a strong geometrical degeneracy between h and N_{eff} at this background level. In principle, also the redshift of recombination depends on h , but this effect is far subdominant [21]. All in all, for the cosmologies close to the Planck bestfit, the combination $H_0 r_s$ scales like³ [21]

$$H_0 r_s \propto \Omega_m^{-0.23} h^{+0.52} N_{\text{eff}}^{-0.1} (\Omega_b h^2)^{-0.11}. \quad (2.4)$$

The determination of $\Omega_b h^2$ (and possibly N_{eff} when it is not equal to 3.044) through BBN and the independent determination of Ω_m from BAO then allow h to be uniquely determined from $H_0 r_s$. However, if the sound horizon r_s is modified through an effect other than through Equation (2.4), then BBN is not sufficient to calibrate it anymore. Naturally, this immediately implies that the BAO+BBN probe loses its constraining power. This is investigated in more depth in Sections 3.7 and 3.8.

²Effects of varying T_{CMB} are discussed in great detail in [44], but since the COBE/FIRAS experiment provides such an excellent measurement of T_{CMB} together with many other experiments, we consider it fixed to 2.7255K for the remainder of this work.

³Instead of from numerical calculations like in [21], the same scaling could also be achieved when considering Eq. (26) of [45] and powerlaw-expanding in the vicinity of the Planck bestfit, giving in Λ CDM $H_0 r_s \propto \Omega_m^{-0.23} h^{0.54} (\Omega_b h^2)^{-0.13}$, which is within the accuracy of the numerical formula. The numerical formula can also be checked easily for extended cosmologies (for example, one can easily find a $m_e^{-0.62}$ scaling relevant for Section 3.8).

2.1.2 Additional probes

Within this work, we will also be making use of unanchored Supernovae of Type Ia from Pantheon[46]/PantheonPLUS[47, 48] as well as Cosmic Chronometer data from [49, 50].

The supernovae of type Ia allow for a measurement of the normalized expansion rate $E(z)$ since the ratio of the observed and intrinsic⁴ luminosities directly determines the product $H_0 D_L(z) = (1+z) \int_0^z [1/E(x)] dx$. This, in turn allows for a direct determination of Ω_m for a flat Λ CDM model, which can aid in the determination of the sound horizon r_s .

The Cosmic Chronometers (CC) method relies on determining the differential age δt and the differential redshifts δz of stellar populations within old massive galaxies that have not undergone strong recent star formation. See the excellent review by [51] for more details. Effectively, CC can thus directly measure the Hubble rate $H(z) \approx -\delta z/\delta t/(1+z)$ and thus, for a given measured normalized expansion rate $E(z)$ also determine the Hubble parameter. These CC measurements are a crucial cross-check of other methods, but – without some additional assumptions – do not yet allow for such a tightly constrained determination of either Ω_m or h alone, which would be needed for a decisive statement about the Hubble tension. Even when combined with other un-anchored late-universe probes, the determination of h is limited by the CC probe – as all other un-anchored probes currently available measure only $E(z)$, not $H(z)$ directly.

2.1.3 ShapeFit

The addition of redshift space distortions (RSD) and in particular the ShapeFit (SF) results are an interesting and novel aspect of this work. While the RSD probe determining the parameter combination $f\sigma_8$ is well known within the literature [41], the SF approach is comparatively new. We refer the reader to [52–54] for a more complete review, and only summarize here the basic features relevant to the BAO+BBN probe. The SF is based on measuring the effective slope of the power spectrum at an intermediate scale of around $0.03h/\text{Mpc}$. This slope is influenced by mainly three effects.

1. The baryon suppression, which is caused by the reduced growth at scales roughly larger than $1/r_s \sim 0.01h/\text{Mpc}$ due to the acoustic oscillations of the baryons preventing their infall in gravitational wells. The amplitude of this suppression is determined through the ratio $[\Omega_b h^2]/[\Omega_m h^2]$.
2. The turnover point of the power spectrum, given by the equality scale k_{eq} , which is determined through the redshift of equality $1+z_{\text{eq}} = [\Omega_m h^2]/\omega_r$.
3. The overall tilt of the power spectrum, which is directly related to the primordial power spectrum tilt n_s .

⁴Naturally these intrinsic luminosities are not measured, but determined through the standardization procedure, by using the parameters of the light curve to estimate this quantity.

Thus, we can see that if SF is calibrated through n_s (from a prior) as well as supplemented through a measurement of $\{\Omega_b h^2, \Omega_m\}$ through the BAO+BBN combination, it can indeed provide an additional measurement of h . This additional constraining power arises from the effects on the matter transfer function of processes around and before the time of matter radiation equality (baryon suppression and turnover).

This method attempts to isolate the information coming from the large, linear scales as compared to the FullModeling analysis⁵ (see for example [55–61]), which relies on perturbative expansions of the power spectrum in order to perform the full modeling of the power spectrum shape. Due to measurements of the broadband shape of the power spectrum, these methods can independently infer H_0 with a relatively high precision (though often they also rely on fixing the baryon density and the primordial spectral index). Particularly, [62] recently showed that by marginalizing over r_s these constraints can be obtained for the Hubble parameter fully independently of the sound horizon information (which is the basis of the BAO+BBN probe) and apply even to extended cosmologies. We will leave a more thorough comparison to FullModeling analyses for future work, but mention that the SF approach has been shown in [53] to provide virtually the same constraining power as FullModeling analyses if similar priors on the primordial spectral index and the baryon density are adopted. The latter, for the purpose of this work, will of course not be necessary and instead will be replaced by the full BBN likelihood (which is further described in [30]).

2.2 Data

We make use of several recent advancements in the measurement of the BAO as well as more precise BBN theoretical predictions from updated interaction rates from the LUNA experiment. We list the data sets we use as well as a short acronym for each below.

- **BAO** We use the newest release of the reconstructed BAO parameters ($\alpha_{\parallel}, \alpha_{\perp}$) from DR16 [41, 63–66], including LRG and QSO. Additionally, this includes high redshift BAO data from the Lyman- α forest⁶ being measured in the DR14 [25, 27]. We also provide a version **BAO (DR12)** that includes older DR12 [67] data instead of the DR16 data. In this combination, the Lyman- α forest data is unchanged.
- **RSD** We use the redshift distortion data measuring the data combination $f\sigma_8$ from the clustering in the newest DR16 data (LRG and QSO) [63–66].
- **SF** We use the measurement of the ShapeFit parameter m from [54]. By default, we also use a prior in $n_s = 0.9637 \pm 0.0044$ motivated from [9] as in the original work.

⁵By this we mean an analysis that uses the full shape of the measured power spectrum for direct inferences on a given model, as opposed to measuring only particular features of it, such as the BAO with $\{\alpha_{\parallel}, \alpha_{\perp}\}$ or the RSD with $\{f\sigma_8\}$.

⁶When this article was at a relatively advanced stage, the Lyman- α forest data from DR16 became public. The difference between DR16 and DR14 Lyman- α forest data is unimportant for the findings of this work (see also Section 3.2).

- **BBN** We use the Big Bang Nucleosynthesis constraints from Aver et al. [35] for Helium and Cooke et al. [34] for Deuterium, using newest theoretical predictions from **Parthenope 3.0** incorporating the LUNA results [38] on the Deuterium-proton to Helium3-photon fusion cross section. We also provide a version **BBN(noLUNA)** that does not include the new theoretical predictions based on the LUNA results, but instead uses older predictions from **Parthenope 2.0** [32].⁷
- **θ_s** We impose a prior ($\theta_s = 1.04109 \pm 0.00030$) on the sound horizon angle as measured by the CMB [9]. This quantity can also be seen as the result of a (massive) data compression process, encoding the angular position of the CMB acoustic peaks; as such this determination is almost entirely model-independent. The model dependence comes in almost exclusively at the interpretation stage.
- **PantheonPLUS** [48] We use the newest compilation of uncalibrated supernovae of Type Ia, constraining $\Omega_m = 0.338 \pm 0.018$ in a flat Λ CDM model. We also provide a version with the older **Pantheon** data [46], which constrains $\Omega_m = 0.298 \pm 0.022$ in a flat Λ CDM model. We use the full likelihoods (not Ω_m priors) in both cases.
- **CC** We use Cosmic Chronometers data from [50], which constrain $H(z)$ by measuring differential ages and redshifts of passive stellar populations within mostly early massive galaxies. We follow the prescription by [50] to include the off-diagonal covariance matrix entries.

For each data combination we run a **MontePython** MCMC chain in order to obtain the corresponding constraints, using **class** as the underlying cosmological code. Unless otherwise stated we require a Gelman-Rubin convergence criterion of $|R-1| < 0.01$ for all parameters to ensure proper convergence of all chains.

3 Results

In Section 3.1 we update the BAO+BBN analysis of [30] to include the new developments in data and modeling discussed in Section 2.2. In Section 3.2 we discuss the contribution to the final constraints coming from different redshifts, and continue in Section 3.3 to investigate the impact of the new ShapeFit results. In Section 3.4 we investigate the addition of a geometric sound horizon angle prior from the CMB and in Sections 3.5 and 3.6 we continue by adding supernovae and cosmic chronometer data. These results of this section initially assume a Λ CDM cosmology, though in Sections 3.7 and 3.8 this Λ CDM assumption will be relaxed in order to check the model-dependence of the BAO+BBN combination. All results are also summarized in Table 1.

⁷In both cases we add a theoretical uncertainty of $6 \cdot 10^{-7}$ for the deuterium abundance, in accordance with [39] for the new rates and approximately with [32] for the old rates. This theoretical uncertainty on deuterium is in decent agreement with the systematic uncertainties from [68]. We also put a 0.0003 theoretical uncertainty for the Helium abundance (as in both [32, 39]), which is propagated from the uncertainty of the neutron lifetime.

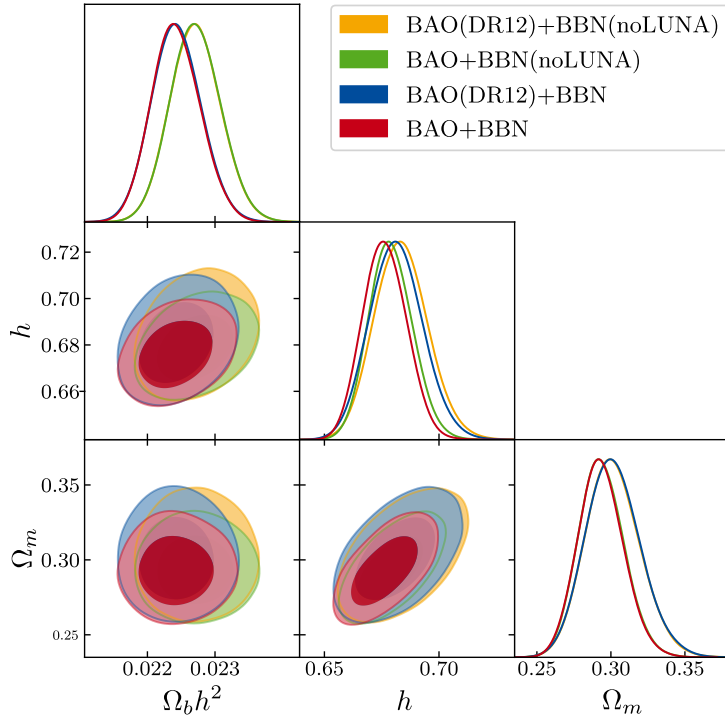


Figure 1. Impact on key parameters in the Λ CDM model of updating the BAO LRG data from DR12 to DR16 and updating the BBN predictions from `Parthenope 2.0` (noLUNA) to LUNA-based theoretical predictions from `Parthenope 3.0`.

3.1 Impact of updated data

We show the impact of updating both the BAO and BBN data on the cosmological parameters constraints in Figure 1.

To quantify the shifts in parameters as well as the change in the uncertainty to a high degree of precision, we require instead $|R - 1| < 10^{-4}$ for these MCMC chains.

There is a shift in $\Omega_b h^2$ from the updated BBN data, as the new theoretical predictions of BBN from `Parthenope 3.0` incorporating the new LUNA results yield a decreased deuterium abundance for a given $\Omega_b h^2$. Due to their anti-correlation, this results in lower values of $\Omega_b h^2$ being preferred in order to give the same measured deuterium abundance. The shift is only at a level of 0.8σ ($\Omega_b h^2 = 0.02272 \pm 0.00038$ with the old predictions vs $\Omega_b h^2 = 0.02242 \pm 0.00037$ with the new LUNA-based predictions), and more importantly does not result in a significant shift of Ω_m (0.02σ). The shift in H_0 (0.3σ) due to the re-calibration of the sound horizon is also rather minor, showing the small dependence of the results on the precise assumed value of $\Omega_b h^2$ from BBN.

Not unexpectedly (given the larger volume surveyed), the new BAO data from DR16 do shift the constraint in Ω_m by around 0.4σ ($\Omega_m = 0.30171 \pm 0.018744$ with DR12 data vs $\Omega_m = 0.29338 \pm 0.015434$ with DR16 data), resulting in a direct shift of H_0 by 0.4σ . We also note that due to the tightening of the constraint on Ω_m by about 20%, the constraint on H_0 is similarly tightened by about 20%.

Taken together, these two effects modify the determination of the Hubble parameter from $H_0 = 68.3_{-1.2}^{+1.1}$ km/s/Mpc for the old analysis to $H_0 = 67.6_{-1.0}^{+0.9}$ km/s/Mpc for the updated analysis, a shift of the constraint of about 0.64σ and a tightening of its uncertainty of about 20%, leading to a total tension of around 3.7σ with the newest Pantheon+SH0ES results from [1] (up from 3.2σ in [30]).

3.2 Impact of internal (in)consistencies

It is well known that the different dependence of r_A on $\{\Omega_m, hr_s\}$ for different redshifts is crucial in aiding the BAO to achieve a tight constraint on Ω_m (as otherwise Ω_m and hr_s would be somewhat degenerate). In [30] we showed that the high- and low-redshift data had quite striking different redshift dependencies (see also [21]), and their intersection happened to lie at a low h value (see Fig. 2 of [30]). At times it has been argued that the low h value preferred by this combination was primarily driven by the internal inconsistency (sometimes even dubbed “tension”, see for example [26]) between the high and low-redshift data sets. This concern was also driven by fears that the Ly α BAO could be impacted by systematics in the modeling of the intergalactic medium (IGM). While [69] shows a great level of consistency across different analyses and data releases, we want to investigate the dependence of our constraint on the high-redshift data and the Ly α BAO in particular.

In Figure 2 we show the resulting constraints from combining BBN data with various subsets of the BAO data.⁸

The results are *largely independent of using BAO measurements from the Lyman- α forest*, as the constraints with and without Lyman- α based BAO almost perfectly overlap. This is different from [30] where the high redshift lever-arm of the Lyman- α data was crucial for obtaining the tight constraints. Now the long lever-arm in redshift offered by the QSO-based BAO mean that the $\Omega_m - hr_s$ (or, with a BBN prior, the $\Omega_m - h$ degeneracy) can be broken even without the information from the Lyman- α forest data (as indicated by the red and blue contours in the left panel of Figure 2).

The 1σ contours of the high-redshift data, both from the QSO alone and from QSO together with the Ly α , now overlap with those of the LRG at lower redshifts (see the dark blue, green, and red contours in Figure 2). This means that *it can no longer be argued that the joint constraint relies on an internal tension* to artificially strengthen the Ω_m constraint (and thus enforce a stricter bound on h).

Note that the data based on the Lyman- α forest do significantly help the QSO determination in the $\Omega_m - h$ degeneracy plane (right panel of Figure 2, green vs dark blue contours), and are perfectly in agreement with the region preferred by the LRG data. This demonstrates again the multiple layers of consistency present in the BAO data, and in particular that *the Lyman- α based data are perfectly compatible with the rest*.

⁸Compare also to fig 5 (right panel) of [41]. We include a few additional sub-divisions of the data, in order to track the differences compared to earlier BAO+BBN combinations.

Finally, part of the reason why the agreement also looks visually better is that the update of DR12 to DR16 LRG data did not only shrink the overall error bars but also slightly shifted the contour towards the region of lower h and Ω_m along the degeneracy direction.

As a consequence, in the following sections we always include the Lyman- α and QSO-based high-redshift BAO data.

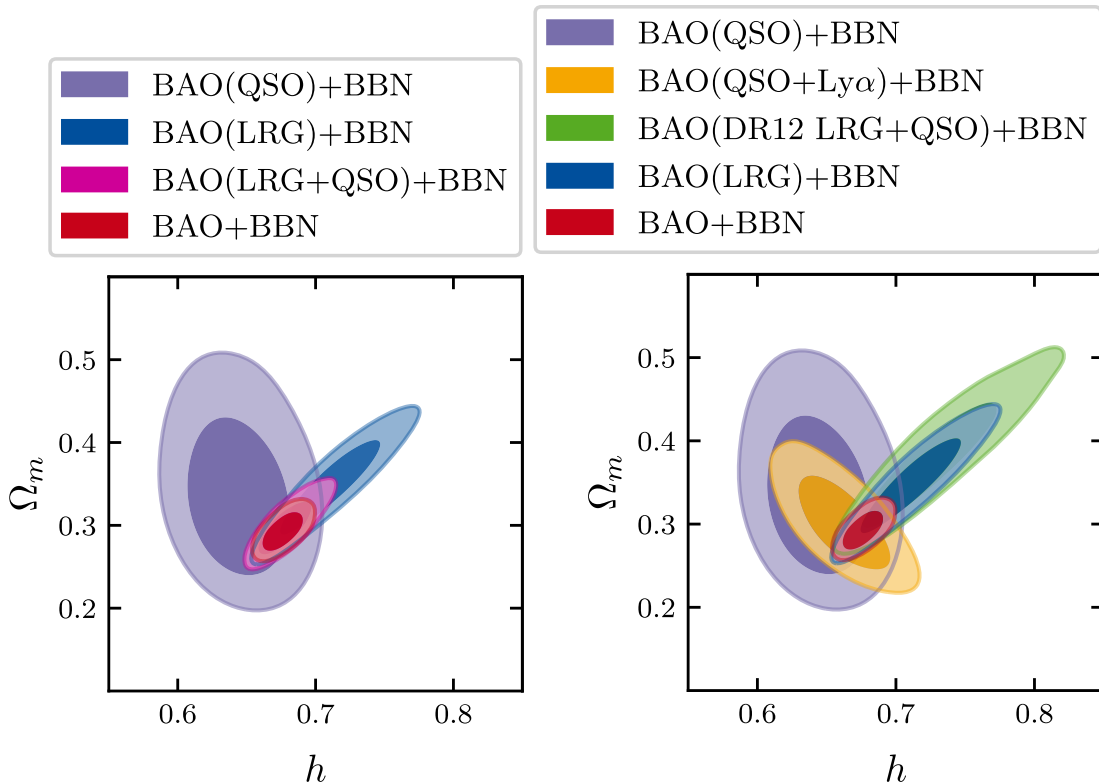


Figure 2. Constraints (in a Λ CDM model) on selected parameters from different subsets of the DR16 BAO data separated by their type – Lyman- α forest based ($\text{Ly}\alpha$), quasar-based (QSO), or based on luminous red galaxies (LRG) compared to the full BAO+BBN probe (LRG+QSO+ $\text{Ly}\alpha$). **Left:** Variations with/without QSO, always without $\text{Ly}\alpha$. **Right:** Variations from including $\text{Ly}\alpha$ or older DR12 BAO data.

3.3 Impact of clustering information beyond BAO

The clustering of tracers of the dark matter can be used beyond the “minimalistic” goal to constrain the classical BAO scaling parameters ($\alpha_{\parallel}, \alpha_{\perp}$) through the measurement of the BAO peak position. Depending on additional assumptions, one can either perform a FullModeling analysis or only include extra information from the RSD (see Section 2.1 for terminology). In the recently-proposed ShapeFit (SF) approach the parameter m is added to the set of parameters in addition to the usual RSD combination $f\sigma_8$, leading to virtually the same constraining power as in the FullModeling analysis (though with increased robustness).

The constraints resulting from including RSD or SF analyses from DR16 LRG are shown in Figure 3. In the top panel we compare the gain in constraining power from RSD and SF data, using the original prescription for both (no prior for RSD, a prior on n_s for SF of $n_s = 0.9637 \pm 0.0044$ motivated by [9]). We see that while the gain in constraining power from RSD is rather minute, SF does significantly shrink the contours. The error bars on h shrink by a factor of 1.3, while the error bars on Ω_m shrink by a factor of 2.0, leading to a measurement of $H_0 = 68.29_{-0.69}^{+0.68}$ km/s/Mpc (3.8σ tension). The reason why SF is expected to give a good additional constraint in the $\{\Omega_m, h\}$ plane is explained in Section 2.1. If we instead drop the prior on n_s for the SF measurement, it loses its constraining power, due to the strong $m - n_s$ degeneracy explained further in [52] and in Section 2.1. We conclude that the SF (with the default n_s prior) strongly supports the existing measurements, while SF without a n_s prior provides no additional constraining power.

As such, we might ask if the RSD constraints would also benefit from a prior on A_s , and this is investigated in the bottom panel of Figure 3. We find that with or without a prior on A_s (here we use $\ln(10^{10}A_s) = 3.047 \pm 0.014$) the constraints on $\{H_0, \Omega_m\}$ are virtually the same. This is because of the strong remaining degeneracy of σ_8 (and thus Ω_m and h) with n_s . Only when including an additional prior on n_s can the RSD provide a small amount of additional constraining power⁹. However, we also notice that the SF measurement is putting much tighter constraints in the $\{H_0, \Omega_m\}$ plane, and the addition of RSD even with the A_s prior (and the default n_s prior of SF) does not lead to a further improvement of the constraints.

Summarizing, a prior on A_s from Planck does not significantly increase the constraining power of the RSD (unlike the n_s prior for SF). Only when including a prior both on A_s and n_s we find that the parameter σ_8 is constrained enough to obtain a competitive inference of Ω_m from RSD, leading to slightly tightened constraints on h for the BAO+BBN combination. However, even this increase in constraining power is much smaller than that obtained from the addition of the SF data. While RSD thus remains an excellent probe of theories of gravity, we find that it is outperformed by the SF on its impact on the Hubble tension.

One can understand why RSD has such a comparatively weak performance¹⁰ compared to BAO and SF in this context as follows. RSD gives constraints on Ω_m (through $f(z)$) which are superseded by the excellent precision of the Ω_m determination from the Alcock-Paczyński effect of the BAO. This holds for any model leaving the late-time expansion history unchanged, as we confirm in Section 3.7.

⁹Of course, this stems from the fact that RSD measure $f\sigma_8$, which, in the limit of a tightly constrained σ_8 , measures mostly Ω_m . In turn, combined with the BAO+BBN probe, this can be converted into a measurement of h .

¹⁰RSD is a very good at detecting mismatches between growth and expansion history, though, and thus is an excellent probe of extended models of gravity beyond general relativity.

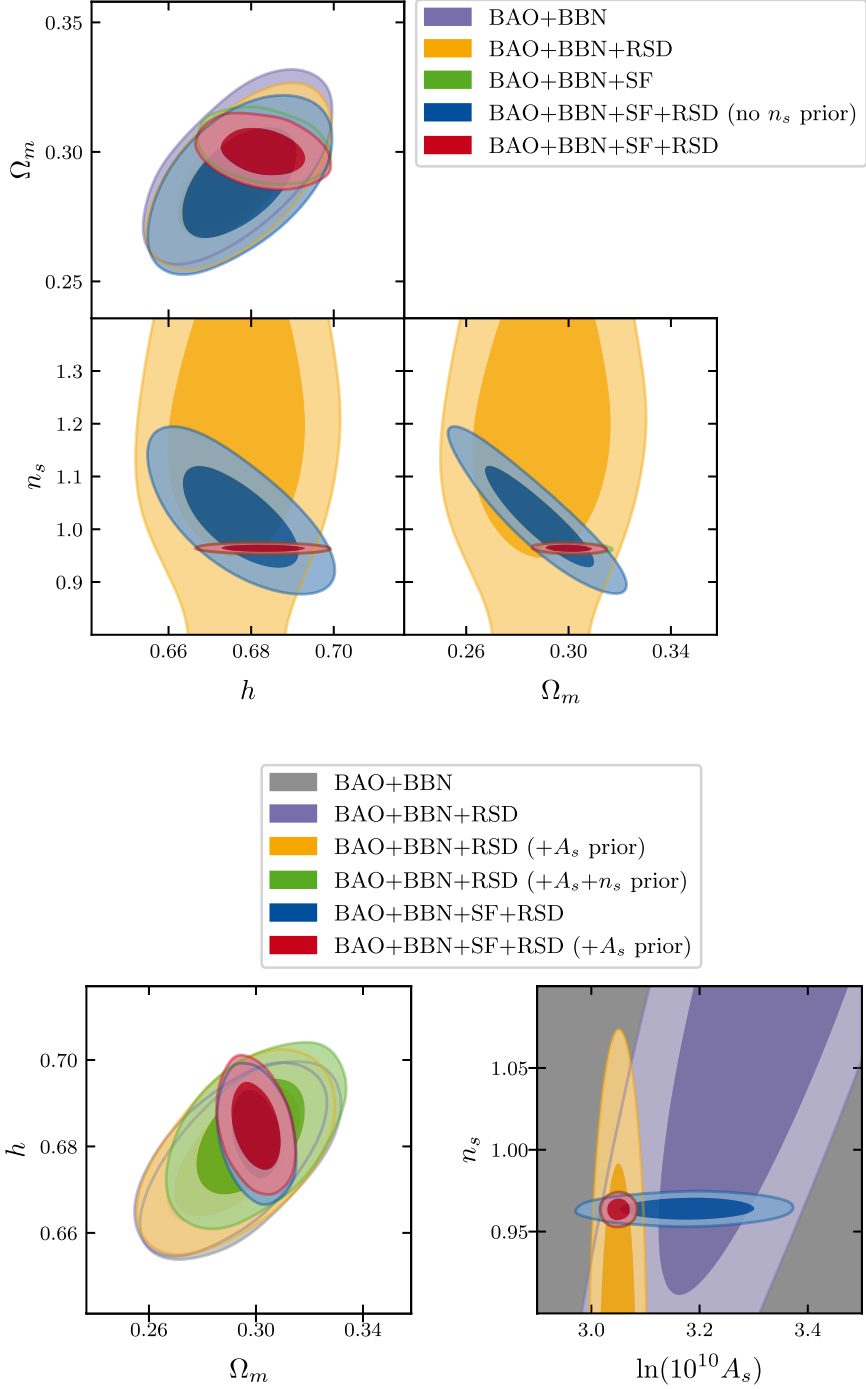


Figure 3. Impact on selected parameters for a Λ CDM model of the redshift space distortion (RSD) and ShapeFit (SF) data (see Section 2.2). Additionally, we impose priors on n_s for the SF by default, and only optionally on A_s and/or n_s for the RSD. **Upper panel:** Combinations of SF with or without n_s prior. Note that the green contours almost perfectly overlap with the red contours, indicating that RSD does not add a lot of information once SF is included. **Lower panel:** Combinations of RSD with various priors on A_s and/or n_s . Only when RSD is combined with both priors (green) are the constraints in h somewhat competitive with those of SF (blue), otherwise overlap with those without RSD (grey/purple/orange).

3.4 Impact of the CMB sound horizon angle

The apparent angular position of the CMB peaks can be measured in an almost model-independent way. The CMB sound horizon angle, θ_s , corresponds almost directly to the location of the various peaks in the angular correlation function, and is thus measured to be about the same value in Λ CDM as well as for models with strong modifications in early or late-time physics. As such, this rather geometric probe can be used as an interesting cross-check. We show the constraints with a prior on θ_s according to Section 2.2 in Figure 4.

The predominant effect of the inclusion of the sound horizon angle information is a much tighter constraint on Ω_m and (through the BBN-calibration of r_s) correspondingly on h . This is to be expected since θ_s has a largely orthogonal dependence on Ω_m compared to the BAO shift parameters due to the large difference in redshift. The mechanism is thus not unlike the way that low and high redshift BAO combine to give a more precise measurement of Ω_m in the first place (see fig. 2 of [30]). In this case, the Ω_m constraint is increased by a factor of 2.5. For a BBN-calibrated r_s this results in a factor of 2.0 for the constraints in h to $H_0 = 68.16 \pm 0.45 \text{ km/s/Mpc}$ (without SF) and $H_0 = 68.30 \pm 0.45 \text{ km/s/Mpc}$ (with SF), leading to an overall tension of 4.2σ (with or without SF). The constraints of the updated BAO+BBN probe together with the geometrical sound horizon information are now as tight as the original analysis of CMB+CMB lensing+BAO was in the original analysis.

We stress that the region of Ω_m preferred by the inclusion of this θ_s prior is the same region of Ω_m preferred by the ShapeFit parameter m (with Planck priors on n_s), suggesting a rather high level of compatibility between these two approaches and consistency of how the model describes the relevant physical processes across widely different epochs in the history of the Universe (BBN, matter-radiation equality, recombination, late-time evolution). Combining the ShapeFit and θ_s results does not lead to a much stronger increase in constraining power since the ShapeFit parameter is just as accurate as the θ_s slice in terms of Ω_m . We can thus expect that upcoming large-scale structure measurements will provide an important consistency check for the Hubble tension at this robust geometrical level.

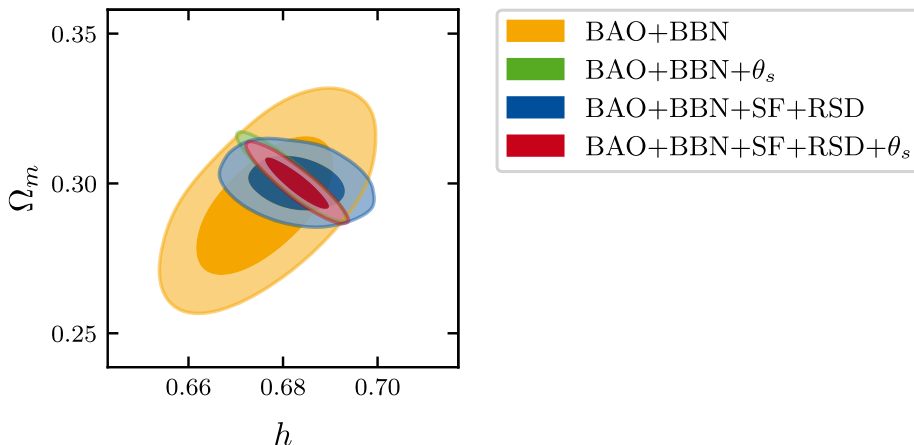


Figure 4. Λ CDM model parameters constraints for BAO+BBN when including a θ_s prior compared to those without. SF denotes ShapeFit, and RSD denotes redshift space distortions. The region preferred by BAO+BBN with a sound horizon prior (green) agrees very well with the region preferred by BAO+BBN with SF+RSD (blue).

3.5 Impact of Pantheon data

Supernovae of type Ia are well known to provide strong constraints on the matter abundance Ω_m even in the absence of an absolute calibration. In Figure 5 we show the impact of including such uncalibrated supernovae using the Pantheon data set. We either show the impact of the updated Pantheon+ data (preferring a slightly higher value of $\Omega_m \approx 0.338 \pm 0.018$ [48]) or the old Pantheon catalogue data (preferring a slightly lower value of $\Omega_m \approx 0.284 \pm 0.012$ [46]). Since the Ω_m value preferred by the updated data set has changed slightly, we show both data sets separately for better comparison with previous literature and for appreciating the effect of this change.

The additional Ω_m constraint from the old Pantheon data is in good agreement with the Ω_m preferred by the combination of BAO measurements, while the new PantheonPLUS data prefers a slightly (around $\sim 1.9\sigma$) higher value. Without SF, the shift in the Hubble parameter caused by this shift in Ω_m is rather minor, leading to $H_0 = 67.75^{+0.70}_{-0.84}$ km/s/Mpc (Pantheon, 4.2σ) or $H_0 = 68.27^{+0.85}_{-0.98}$ km/s/Mpc (PantheonPLUS, 3.5σ). The corresponding (perhaps unexpected) decrease in constraining power for PantheonPLUS compared to the old Pantheon data is naturally explained by the discrepancy in the singular Ω_m constraints with BAO in PantheonPLUS, leading to widened combined constraints (which propagate to widened constraints on $H_0 r_s$ and thus on h). If we instead include SF data, the results are remarkably stable and no significant shift in H_0 is observed.

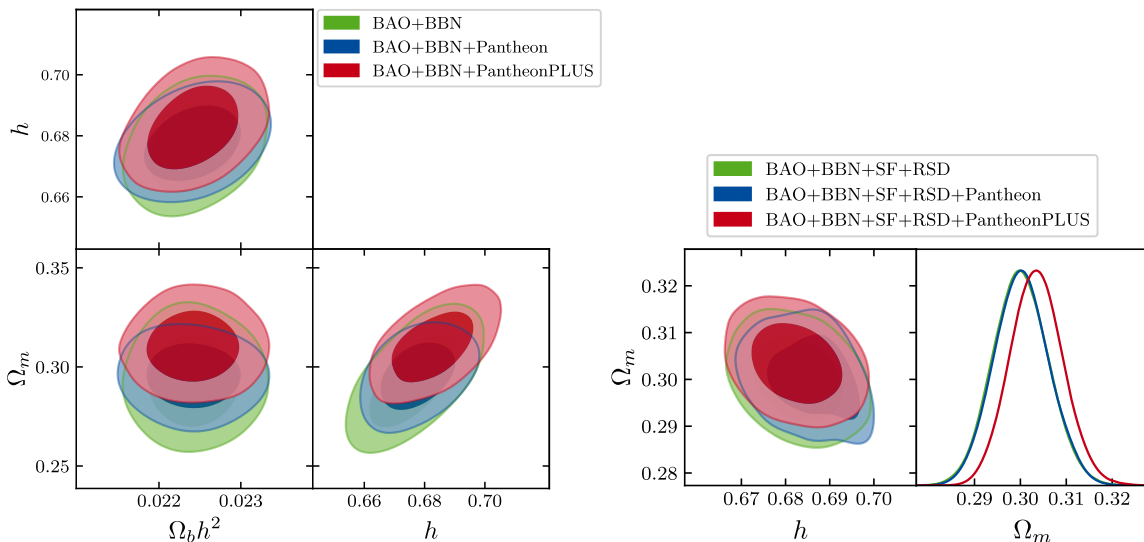


Figure 5. Impact of including old Pantheon or new Pantheon+ (PantheonPLUS) data on selected parameters constraints for a Λ CDM model. SF denotes ShapeFit, and RSD denotes redshift space distortions. **Left:** Without using any SF or RSD data. There is no significant change in $\Omega_b h^2$ between the data sets. **Right:** Including SF and RSD data. We also show the 1D posterior on Ω_m , which shows a slight shift for PantheonPLUS compared to the analysis without it.

3.6 Impact of Cosmic Chronometer Data

The cosmic chronometers (CC) are an excellent late-universe probe for both Ω_m and more directly H_0 due to their direct measurement of $H(z)$. We show the corresponding results in Figure 6. We find that the addition of CC is mostly relevant when not including SF or RSD data, since, in this context, those supersede the constraining power of the CC. As a result, the CC can make the measurement more robust, but do not strengthen the constraint a lot by themselves. For the combination without SF and RSD we see a small decrease of the error bars of Ω_m and h by 9% each.

We also show the combination of PantheonPLUS and CC data, where we observe a small increase of constraining power due to the PantheonPLUS, especially in the case without SF or RSD data. There is a mild synergy between the two added data sets, achieving a decrease in the error bars of around 9% in Ω_m and 16% in h compared to the result when only including PantheonPLUS data. This is because the CC data prevent an upward shift in Ω_m and h as seen in Figure 5, caused by the slightly higher value of Ω_m in the PantheonPLUS data.

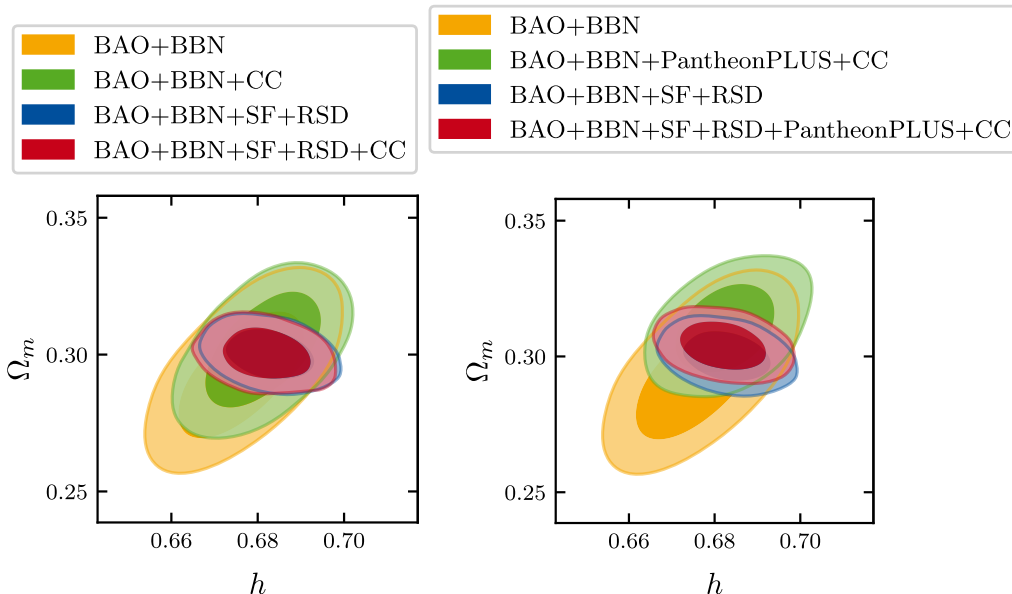


Figure 6. Impact of including cosmic chronometers (CC) data with and without PantheonPLUS data (always for a Λ CDM model). SF denotes ShapeFit, and RSD denotes redshift space distortions. **Left:** Without PantheonPLUS data. **Right:** With PantheonPLUS data.

3.7 The BAO+BBN probe with dark radiation

Dark radiation can change the expansion rate in the early Universe, thus impacting the scale of the sound horizon (see Equations (2.2) to (2.4)). Due to the $H_0 - r_s$ degeneracy, the presence of dark radiation strongly affects the H_0 determination from both the CMB and the BAO+BBN probe. The latter, in particular, is sensitive to any additional dark radiation at the time of the BBN, through the increased expansion rate, which in turns affect the light elements abundance.

As such, the BAO+BBN probe can give independent and very relevant constraints for N_{eff} and h in a way that does not depend on the precise Silk-damping mechanics of the dark radiation (which is very important for the CMB, see e.g. [17]). It is worth noting, however, that such constraints on N_{eff} can be avoided when considering a boost/production of the dark radiation abundance only after BBN. In Figure 7 we show the results both with and without BBN, in order to exemplify the importance of BBN in the constraints obtained for this model.

For the BAO+BBN probe, the addition of N_{eff} does cause a widening of the constraints on the $\Omega_m - h$ plane, independently of whether SF/RSD data is included or not¹¹. This is because the $H_0 - r_s$ degeneracy can only be partially broken in this model¹², allowing for only comparatively weaker constraints on H_0 after marginalizing over allowed values N_{eff} and the corresponding values of r_s . We note that the results are different from [54], which used a BBN-motivated prior on $\Omega_b h^2$ instead of the full BBN likelihood used in this work, which primarily makes a difference for models of dark radiation that are constrained in this work by their impact on the Y_p primordial abundance.

Instead, when abandoning the BBN constraints on this model altogether, both $\Omega_b h^2$ and N_{eff} become unconstrained, as expected from Section 2.1, leading to no constraint in h (except due to prior bounds). Interestingly, the improved constraint of Ω_m from SF present in Λ CDM is also relaxed in the N_{eff} model without BBN. This is because the calibration of the Ω_m is of course an indirect result of the SF only possible when $\Omega_b h^2$ is sufficiently fixed (which it isn't without BBN), as otherwise the inherent degeneracies in the measurement of m make precise inference of h or Ω_m from SF alone impossible. Thus, only the Alcock-Paczyński-based BAO measurement of Ω_m remains.

It is worth mentioning that also in this extended model RSD does not provide additional information compared to the BAO (the contours are identical to those displayed in the left panel of Figure 7), as explained in Section 3.3.

In Figure 8 we also show that for the model including dark radiation one still obtains constraints of similar strength on the Hubble parameter h when adding an angular sound horizon prior from the CMB compared to those of adding FS+RSD. More importantly, however, the BAO+BBN probe can – in combination with the RSD+FS data – constrain exactly this sound horizon angular scale very precisely (orange/red contour of Figure 8) and the value inferred is very well in agreement with that from the CMB (green contour of Figure 8), providing yet another crucial cross-check/consistency test. Applications of this cross-check to other models is left for future work.

¹¹Compared to the Λ CDM model, without SF+RSD the constraints widen by a factor of around 2, to $H_0 = 66.81^{+1.95}_{-1.93}$ km/s/Mpc. Instead, with SF+RSD the constraints widen by a factor of around 2.5, to $H_0 = 67.89^{+1.75}_{-1.80}$ km/s/Mpc.

¹²This is because there remains a $\{\Omega_b h^2, N_{\text{eff}}\}$ degeneracy in BBN constraints, as an increase in $\Omega_b h^2$ can be partially compensated by an increase in N_{eff} while keeping the Deuterium abundance the same (see e.g. Fig 1 of [30]). Only when the N_{eff} becomes too large and starts to perturb the Y_p measurement significantly, is this degeneracy broken, thus leading to overall much weaker constraints on $\Omega_b h^2$ in this model, allowing for additional freedom in r_s .

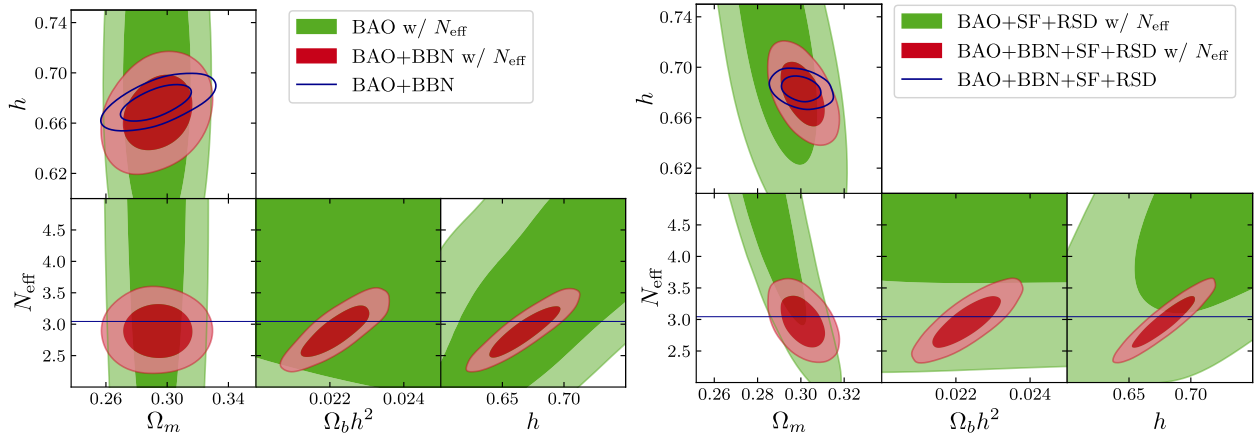


Figure 7. Constraints of the model including additional dark radiation through N_{eff} . SF denotes ShapeFit, and RSD denotes redshift space distortions. For reference, the solid blue lines correspond to the results in the Λ CDM model. **Left:** Without SF+RSD data. **Right:** With SF+RSD data.

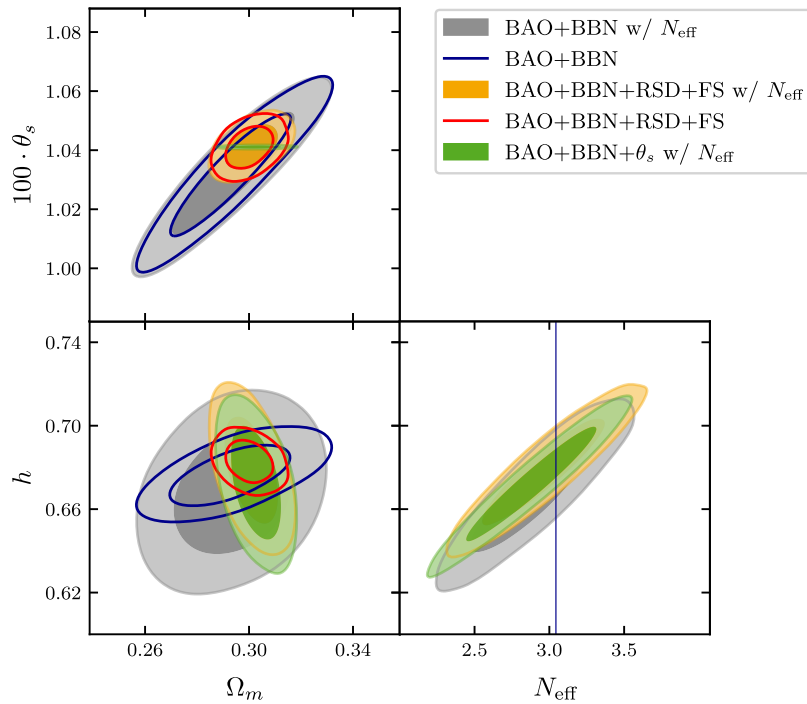


Figure 8. Constraints of the model including additional dark radiation through N_{eff} as well as a prior on θ_s (green contour), compared to various other constraints (other contours). SF denotes ShapeFit, and RSD denotes redshift space distortions. For reference, the solid blue lines and the solid red lines correspond to the results in the Λ CDM model. The top left panel shows that the value of $100 \cdot \theta_s$ inferred from the FS+RSD addition to BAO+BBN is very well in agreement with the sound horizon prior as measured from the CMB.

3.8 The BAO+BBN probe with shifted recombination

Another possibility to shift the sound horizon at recombination is by changing the redshift of recombination. While several models have been proposed, in this work we focus on a model of a varying electron mass m_e due to its simplicity. For this particular model, by investigating a few test cases, [70] has shown that BBN can in principle provide tight constraints. Here we extend that discussion by performing a fully Bayesian analysis using the BBN likelihood of [30] with the prescription for including the electron mass as in [70].¹³ The constraints are shown in the right panel of Figure 9.

However, we will also be more generally interested in treating this model as an effective toy model that produces shifts of the recombination redshift, which can also be accomplished by other mechanisms (such as [43]). In this more general context, we will begin by explicitly assuming the variation of the electron mass to be caused by a physical effect only after the times relevant for BBN. This will allow us to draw conclusions about models that shift the sound horizon of recombination without leaving an impact on BBN. We show the corresponding constraints in the left panel of Figure 9.

In the case that the variation does not leave an impact on BBN (left panel of Figure 9), we see that the constraints on the varying electron mass model are quite loose. We find that without SF or RSD data the Hubble parameter remains unconstrained, as the model-induced degeneracy between the varying electron mass and h is perfect. Without the calibration of r_s through BBN, the BAO+BBN probe cannot constrain H_0 anymore (except for the bounds from the prior). Instead, if SF data are added, weak constraints on h are actually recovered. These stem from the $\{\omega_b, n_s\}$ -calibrated measurement of the parameter m , which does allow for a joint measurement of approximately $\Omega_m h^2 \approx \text{const}$. This demonstrates that, although currently not competitive with the BAO+BBN-derived constraints in ΛCDM , the SF does add valuable and independent information, which becomes especially important in extended models. We expect that such a result remains true for other extended models, but leave a more detailed investigation for future work. This discussion is expected to also apply to models that shift the sound horizon through an increase in the expansion rate between BBN and recombination, which also shifts r_s in a way that does not impact BBN, and thus leads to the same effects as discussed above. Note, however, that in this case we expect that the interpretation of the SF parameter needs to be adjusted accordingly. We leave the detailed investigation of the SF constraint on such models modifying the expansion rate before recombination to future work.

In the case that we allow the varying m_e - model to be constrained by BBN (right panel of Figure 9), we naturally find much tighter constraints. Indeed, we see that the constraints on m_e are driven by BBN alone, and consequently a similar indirect calibration of the sound horizon as in Section 3.7 is possible. In this case, the BAO+BBN probe by itself only gives relatively weak constraints on h .

¹³This prescription only adjusts the neutron decay rate (see eq. 3 of [70]), but this is expected to be the dominant effect on BBN. We leave a full implementation of the variation of other rates to future work.

Similarly to Section 3.7 we find that the SF constraints in this case add a lot of additional constraining power due to their tight $\{\Omega_m, h\}$ correlation, though naturally the constraints are weaker than that of Λ CDM. Interestingly, they are still stronger than those in Λ CDM without SF (red line in Figure 9, right panel).

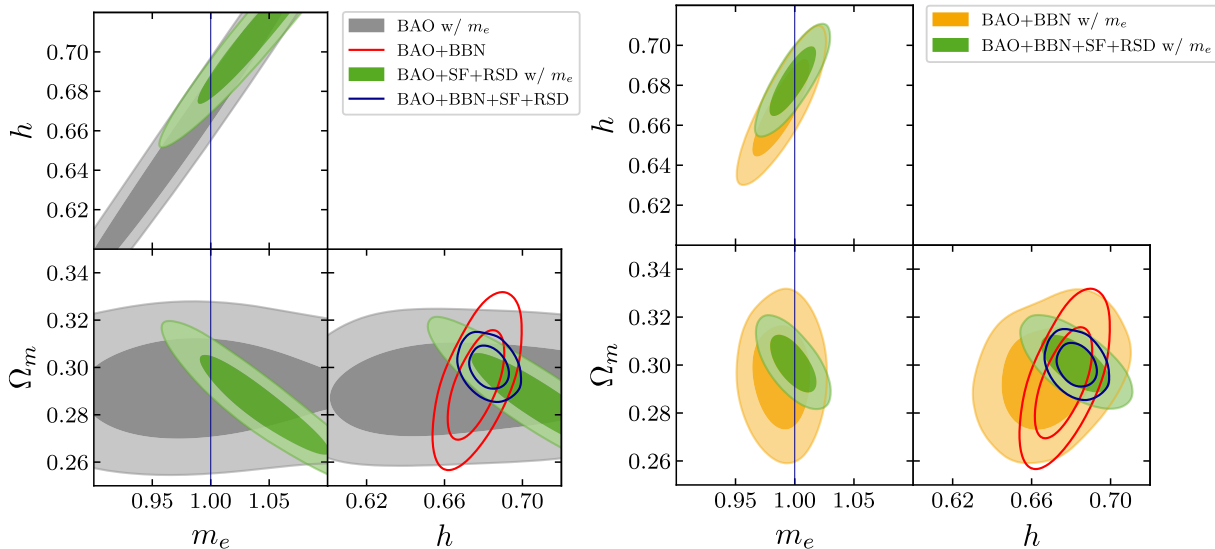


Figure 9. Constraints for the BAO+BBN probe for the model of including additional variation of the redshift of recombination through a variation of the electron mass (m_e). The parameter m_e is shown relative to the value measured today (511keV). SF denotes ShapeFit, and RSD denotes redshift space distortions. **Left:** Not including the impact of the model on BBN. **Right:** Including the impact of the model on BBN.

4 Conclusions

The BAO+BBN probe has been shown to provide an excellent background probe of the expansion rate of the Universe. With the new results from the LUNA experiment [38] as well as the latest data release DR16 of SDSS [41, 42] an update of the results is timely. More importantly, this gives us the occasion to investigate several additional aspects of this probe, such as combinations with a variety of additional measurements, and the robustness to the choice of the underlying cosmological model.

First and foremost, we find that the new data put very tight constraints on the Hubble parameter without relying on CMB data: $H_0 = 67.6^{+0.9}_{-1.0}$ km/s/Mpc in Λ CDM, which breaches the 1km/s/Mpc mark recently achieved by local distance ladder determinations [1]. This represents a tightening of the constraint by roughly 20% and a 0.6σ downward shift from the result in [30], $H_0 = 68.3^{+1.1}_{-1.2}$ km/s/Mpc. The Gaussian tension (GT) with the newest PantheonPLUS+SH0ES result [1] has thus grown from 3.2σ to 3.7σ .

Secondly, there is no longer any reliance on datasets that carry a mild internal tension at the 2σ level. It is worth noting that the increased precision is possible even without the highest redshift data used in this work ($\text{Ly}\alpha$ from DR14) due to the statistical power of the DR16 measurement of the BAO in QSO already providing sufficient lever arm to break the degeneracy between $H_0 r_s$ and Ω_m . We explicitly mention that we do not find any discrepancy of the $\text{Ly}\alpha$ data from the other data sets.

Third, we investigated the addition of other features that can be extracted from the clustering data, such as the redshift space distortion (RSD) constraints on the parameter combination $f\sigma_8$ or the ShapeFit (SF) constraints on the parameter m . Especially the latter is very synergistic with the BAO+BBN measurement (if a prior on n_s is included), leading to competitively tight constraints at the level of $H_0 = 68.3 \pm 0.7 \text{ km/s/Mpc}$ (3.8σ GT). Instead, RSD does not add a lot of synergistic information to the BAO+BBN measurement in terms of the Hubble tension, and leads to essentially the same constraints as without (even with a prior on A_s imposed).

Fourth, we investigate how the constraints from the BAO+BBN probe improve if other synergistic geometrical background data are added to it. The early Universe angular sound horizon of the BAO observed in the CMB (θ_s) is measured at sub-percent precision (0.03%) in an almost model-independent way. With only this additional information from the CMB, the precision of the BAO+BBN probe reaches the same level as the original CMB+CMB lensing+BAO analysis in [9], reaching $H_0 = 68.2 \pm 0.45 \text{ km/s/Mpc}$ (4.2σ GT). More importantly, the region in parameter space preferred by this combination is perfectly in agreement with that preferred by adding the SF measurement. If we instead add Pantheon data, we also notice a slight increment of the constraining power, comparable to that when the SF data are added. Since the newest PantheonPLUS [48] has a slightly different bestfit ($\sim 1.9\sigma$) for Ω_m from the BAO data, the results are different compared to the addition of the older Pantheon data [46], leading either to $H_0 = 67.8^{+0.7}_{-0.8} \text{ km/s/Mpc}$ (Pantheon, 4.2σ GT) or $H_0 = 68.3^{+0.9}_{-1.0}$ (PantheonPLUS, 3.5σ GT). The addition of Cosmic Chronometer (CC) data decrease the uncertainties slightly (by $\sim 9\%$), and does prefer the same region in parameter space, again demonstrating the nice consistency between the probes.

Finally, we investigate the model-dependence of the BAO+BBN constraints with respect to early-time solutions of the Hubble tension. We show that models of dark radiation or a varied electron mass are constrained by BBN. The resulting constraints are degraded only by a factor of 2 compared to the ΛCDM model (and are tighter than when only a $\Omega_b h^2$ prior is included as in [54]). This is expected to generalize for other models that can be constrained with BBN. A comparison with [62] highlights this strong impact of the BBN probe on the allowed parameter regions of the N_{eff} and m_e models: Upon inclusion of BBN constraints we find that the Hubble tension with the SH0ES results increases to 2.8σ GT (N_{eff}) and 3.5σ GT (m_e), respectively. On the other hand, models that purely shift the sound horizon at recombination without measurable impact on the BBN are expected not to be bounded by the BAO+BBN probe, though the additional information from SF provides hope for constraints in the near future.

We conclude that the BAO+BBN combination is an incredibly interesting and constraining probe of the geometrical expansion history of the universe and the Hubble tension, especially when combined with the ShapeFit measurement as described in [52, 54] to give a 0.7km/s/Mpc determination of the Hubble parameter. Even further, the BAO+BBN probe profits quite dramatically from combinations with other geometric probes, such as the angular sound horizon of the CMB, uncalibrated standardized supernovae of type Ia, or Cosmic Chronometers. In particular, all inferences of the Hubble parameter from these various combinations agree on the inferred Hubble parameter and agree with the determination from the CMB anisotropies. Finally, we show that with a word of caution there is a dependence of the BAO+BBN probe on the assumed underlying model, if it modifies the early-time expansion history. While constraints can be obtained for models that have an impact on the BBN, no inference on the Hubble parameter can be made for other models. However, we find a hint that the addition of a precise shape measurement could provide important independent constraints on these models.

In the future new data from ongoing and upcoming large scale structure surveys will most definitely make the BAO+BBN probe together with its SF and RSD additions one of the most interesting cosmological probes of modern cosmology, providing a crucial cross-check of the results derived from the CMB and the local distance ladder. This will also allow to shed new light on the proposed theoretical solutions to the Hubble tension.

Acknowledgments

We would like to thank Vivian Poulin for providing the PantheonPLUS likelihood and helpful discussions. We would further like to thank Raul Jimenez for pointing out several works providing a critical discussion on Lyman- α based BAO data, sparking the idea for Section 3.2 as a response. We would also like to thank Julien Lesgourgues for helpful comments and a detailed discussion on BBN theoretical uncertainties. Finally, we would like to thank Guillermo Franco Abellán for his comments. Funding for this work was provided by project PGC2018-098866-B-I00 MCIN/AEI/10.13039/501100011033 y FEDER “Una manera de hacer Europa”, as well as the “Center of Excellence Maria de Maeztu 2020-2023” award to the ICC University Barcelona (CEX2019-000918-M funded by MCIN/AEI/10.13039/501100011033) and European Union’s Horizon 2020 research and innovation programme ERC (BePreSysE, grant agreement 725327).

References

- [1] A. G. Riess et al., *A Comprehensive Measurement of the Local Value of the Hubble Constant with $1\text{ km s}^{-1}\text{ Mpc}^{-1}$ Uncertainty from the Hubble Space Telescope and the SH0ES Team*, *Astrophys. J. Lett.* **934** (2022), no. 1 L7, [[arXiv:2112.04510](#)].
- [2] W. L. Freedman et al., *The Carnegie-Chicago Hubble Program. VIII. An Independent Determination of the Hubble Constant Based on the Tip of the Red Giant Branch*, [[arXiv:1907.05922](#)].

- [3] W. L. Freedman, B. F. Madore, T. Hoyt, I. S. Jang, R. Beaton, M. G. Lee, A. Monson, J. Neeley, and J. Rich, *Calibration of the Tip of the Red Giant Branch (TRGB)*, [arXiv:2002.01550](#).
- [4] G. S. Anand, R. B. Tully, L. Rizzi, A. G. Riess, and W. Yuan, *Comparing Tip of the Red Giant Branch Distance Scales: An Independent Reduction of the Carnegie-Chicago Hubble Program and the Value of the Hubble Constant*, *Astrophys. J.* **932** (2022), no. 1 15, [[arXiv:2108.00007](#)].
- [5] W. L. Freedman, *Measurements of the Hubble Constant: Tensions in Perspective*, *Astrophys. J.* **919** (2021), no. 1 16, [[arXiv:2106.15656](#)].
- [6] E. Abdalla et al., *Cosmology intertwined: A review of the particle physics, astrophysics, and cosmology associated with the cosmological tensions and anomalies*, *JHEAp* **34** (2022) 49–211, [[arXiv:2203.06142](#)].
- [7] E. Di Valentino, O. Mena, S. Pan, L. Visinelli, W. Yang, A. Melchiorri, D. F. Mota, A. G. Riess, and J. Silk, *In the realm of the Hubble tension—a review of solutions*, *Class. Quant. Grav.* **38** (2021), no. 15 153001, [[arXiv:2103.01183](#)].
- [8] L. Verde, T. Treu, and A. G. Riess, *Tensions between the Early and the Late Universe*, *Nature Astron.* **3** (7, 2019) 891, [[arXiv:1907.10625](#)].
- [9] **Planck** Collaboration, N. Aghanim et al., *Planck 2018 results. VI. Cosmological parameters*, *Astron. Astrophys.* **641** (2020) A6, [[arXiv:1807.06209](#)]. [Erratum: *Astron. Astrophys.* 652, C4 (2021)].
- [10] **ACT** Collaboration, S. Aiola et al., *The Atacama Cosmology Telescope: DR4 Maps and Cosmological Parameters*, *JCAP* **12** (2020) 047, [[arXiv:2007.07288](#)].
- [11] **SPT-3G** Collaboration, D. Dutcher et al., *Measurements of the E-mode polarization and temperature-E-mode correlation of the CMB from SPT-3G 2018 data*, *Phys. Rev. D* **104** (2021), no. 2 022003, [[arXiv:2101.01684](#)].
- [12] W. L. Freedman, *Cosmology at a Crossroads*, *Nature Astron.* **1** (2017) 0121, [[arXiv:1706.02739](#)].
- [13] **Planck** Collaboration, P. A. R. Ade et al., *Planck 2013 results. XVI. Cosmological parameters*, *Astron. Astrophys.* **571** (2014) A16, [[arXiv:1303.5076](#)].
- [14] A. G. Riess et al., *A 2.4% Determination of the Local Value of the Hubble Constant*, *Astrophys. J.* **826** (2016), no. 1 56, [[arXiv:1604.01424](#)].
- [15] J. L. Bernal, L. Verde, and A. G. Riess, *The trouble with H_0* , *JCAP* **10** (2016) 019, [[arXiv:1607.05617](#)].
- [16] L. Verde, P. Protopapas, and R. Jimenez, *Planck and the local Universe: Quantifying the tension*, *Phys. Dark Univ.* **2** (2013) 166–175, [[arXiv:1306.6766](#)].
- [17] N. Schöneberg, G. Franco Abellán, A. Pérez Sánchez, S. J. Witte, V. Poulin, and J. Lesgourgues, *The H_0 Olympics: A fair ranking of proposed models*, *Phys. Rept.* **984** (2022) 1–55, [[arXiv:2107.10291](#)].
- [18] L. Perivolaropoulos and F. Skara, *Challenges for Λ CDM: An update*, *New Astron. Rev.* **95** (2022) 101659, [[arXiv:2105.05208](#)].

- [19] K. Aylor, M. Joy, L. Knox, M. Millea, S. Raghunathan, and W. L. K. Wu, *Sounds Discordant: Classical Distance Ladder & Λ CDM -based Determinations of the Cosmological Sound Horizon*, *Astrophys. J.* **874** (2019), no. 1 4, [[arXiv:1811.00537](#)].
- [20] L. Knox and M. Millea, *Hubble constant hunter’s guide*, *Phys. Rev. D* **101** (2020), no. 4 043533, [[arXiv:1908.03663](#)].
- [21] N. Schöneberg, *Anomalies in cosmological data and probes of the dark sector*. PhD thesis, RWTH Aachen U., 2021.
- [22] G. E. Addison, G. Hinshaw, and M. Halpern, *Cosmological constraints from baryon acoustic oscillations and clustering of large-scale structure*, *Mon. Not. Roy. Astron. Soc.* **436** (2013) 1674–1683, [[arXiv:1304.6984](#)].
- [23] E. Aubourg et al., *Cosmological implications of baryon acoustic oscillation measurements*, *Phys. Rev. D* **92** (2015), no. 12 123516, [[arXiv:1411.1074](#)].
- [24] G. E. Addison, D. J. Watts, C. L. Bennett, M. Halpern, G. Hinshaw, and J. L. Weiland, *Elucidating Λ CDM: Impact of Baryon Acoustic Oscillation Measurements on the Hubble Constant Discrepancy*, *Astrophys. J.* **853** (2018), no. 2 119, [[arXiv:1707.06547](#)].
- [25] M. Blomqvist et al., *Baryon acoustic oscillations from the cross-correlation of Ly α absorption and quasars in eBOSS DR14*, *Astron. Astrophys.* **629** (2019) A86, [[arXiv:1904.03430](#)].
- [26] A. Cuceu, J. Farr, P. Lemos, and A. Font-Ribera, *Baryon Acoustic Oscillations and the Hubble Constant: Past, Present and Future*, *JCAP* **10** (2019) 044, [[arXiv:1906.11628](#)].
- [27] V. de Sainte Agathe et al., *Baryon acoustic oscillations at $z = 2.34$ from the correlations of Ly α absorption in eBOSS DR14*, *Astron. Astrophys.* **629** (2019) A85, [[arXiv:1904.03400](#)].
- [28] **BOSS** Collaboration, A. Font-Ribera et al., *Quasar-Lyman α Forest Cross-Correlation from BOSS DR11 : Baryon Acoustic Oscillations*, *JCAP* **05** (2014) 027, [[arXiv:1311.1767](#)].
- [29] **BOSS** Collaboration, T. Delubac et al., *Baryon acoustic oscillations in the Ly α forest of BOSS DR11 quasars*, *Astron. Astrophys.* **574** (2015) A59, [[arXiv:1404.1801](#)].
- [30] N. Schöneberg, J. Lesgourgues, and D. C. Hooper, *The BAO+BBN take on the Hubble tension*, *JCAP* **10** (2019) 029, [[arXiv:1907.11594](#)].
- [31] O. Pisanti, A. Cirillo, S. Esposito, F. Iocco, G. Mangano, G. Miele, and P. D. Serpico, *PARthENoPE: Public Algorithm Evaluating the Nucleosynthesis of Primordial Elements*, *Comput. Phys. Commun.* **178** (2008) 956–971, [[arXiv:0705.0290](#)].
- [32] R. Consiglio, P. F. de Salas, G. Mangano, G. Miele, S. Pastor, and O. Pisanti, *PARthENoPE reloaded*, *Comput. Phys. Commun.* **233** (2018) 237–242, [[arXiv:1712.04378](#)].
- [33] C. Pitrou, A. Coc, J.-P. Uzan, and E. Vangioni, *Precision big bang nucleosynthesis with improved Helium-4 predictions*, *Phys. Rept.* **754** (2018) 1–66, [[arXiv:1801.08023](#)].
- [34] R. J. Cooke, M. Pettini, and C. C. Steidel, *One Percent Determination of the Primordial Deuterium Abundance*, *Astrophys. J.* **855** (2018), no. 2 102, [[arXiv:1710.11129](#)].
- [35] E. Aver, K. A. Olive, and E. D. Skillman, *The effects of He I λ 10830 on helium abundance determinations*, *JCAP* **07** (2015) 011, [[arXiv:1503.08146](#)].
- [36] A. Peimbert, M. Peimbert, and V. Luridiana, *The primordial helium abundance and the number of neutrino families*, *Rev. Mex. Astron. Astrofis.* **52** (2016), no. 2 419–424, [[arXiv:1608.02062](#)].

- [37] Y. I. Izotov, T. X. Thuan, and N. G. Guseva, *A new determination of the primordial He abundance using the He I $\lambda 10830 \text{ \AA}$ emission line: cosmological implications*, *Mon. Not. Roy. Astron. Soc.* **445** (2014), no. 1 778–793, [[arXiv:1408.6953](#)].
- [38] V. Mossa et al., *The baryon density of the Universe from an improved rate of deuterium burning*, *Nature* **587** (2020), no. 7833 210–213.
- [39] S. Gariazzo, P. F. de Salas, O. Pisanti, and R. Consiglio, *PARthENoPE revolutions*, *Computer Physics Communications* **271** (Feb., 2022) 108205, [[arXiv:2103.05027](#)].
- [40] C. Pitrou, A. Coc, J.-P. Uzan, and E. Vangioni, *Precision Big Bang Nucleosynthesis with the New Code PRIMAT*, *JPS Conf. Proc.* **31** (2020) 011034, [[arXiv:1909.12046](#)].
- [41] **eBOSS** Collaboration, S. Alam et al., *Completed SDSS-IV extended Baryon Oscillation Spectroscopic Survey: Cosmological implications from two decades of spectroscopic surveys at the Apache Point Observatory*, *Phys. Rev. D* **103** (2021), no. 8 083533, [[arXiv:2007.08991](#)].
- [42] **SDSS-IV** Collaboration, R. Ahumada et al., *The 16th Data Release of the Sloan Digital Sky Surveys: First Release from the APOGEE-2 Southern Survey and Full Release of eBOSS Spectra*, *Astrophys. J. Suppl.* **249** (2020), no. 1 3, [[arXiv:1912.02905](#)].
- [43] K. Jedamzik and L. Pogosian, *Relieving the Hubble tension with primordial magnetic fields*, *Phys. Rev. Lett.* **125** (2020), no. 18 181302, [[arXiv:2004.09487](#)].
- [44] M. M. Ivanov, Y. Ali-Haïmoud, and J. Lesgourgues, *H0 tension or T0 tension?*, *Phys. Rev. D* **102** (2020), no. 6 063515, [[arXiv:2005.10656](#)].
- [45] D. J. Eisenstein and W. Hu, *Baryonic features in the matter transfer function*, *Astrophys. J.* **496** (1998) 605, [[astro-ph/9709112](#)].
- [46] **Pan-STARRS1** Collaboration, D. M. Scolnic et al., *The Complete Light-curve Sample of Spectroscopically Confirmed SNe Ia from Pan-STARRS1 and Cosmological Constraints from the Combined Pantheon Sample*, *Astrophys. J.* **859** (2018), no. 2 101, [[arXiv:1710.00845](#)].
- [47] D. Scolnic et al., *The Pantheon+ Analysis: The Full Dataset and Light-Curve Release*, [[arXiv:2112.03863](#)].
- [48] D. Brout et al., *The Pantheon+ Analysis: Cosmological Constraints*, [[arXiv:2202.04077](#)].
- [49] M. Moresco, R. Jimenez, L. Verde, L. Pozzetti, A. Cimatti, and A. Citro, *Setting the Stage for Cosmic Chronometers. I. Assessing the Impact of Young Stellar Populations on Hubble Parameter Measurements*, *Astrophys. J.* **868** (2018), no. 2 84, [[arXiv:1804.05864](#)].
- [50] M. Moresco, R. Jimenez, L. Verde, A. Cimatti, and L. Pozzetti, *Setting the Stage for Cosmic Chronometers. II. Impact of Stellar Population Synthesis Models Systematics and Full Covariance Matrix*, *Astrophys. J.* **898** (2020), no. 1 82, [[arXiv:2003.07362](#)].
- [51] M. Moresco et al., *Unveiling the Universe with Emerging Cosmological Probes*, [[arXiv:2201.07241](#)].
- [52] S. Brieden, H. Gil-Marín, and L. Verde, *ShapeFit: extracting the power spectrum shape information in galaxy surveys beyond BAO and RSD*, *JCAP* **12** (2021), no. 12 054, [[arXiv:2106.07641](#)].
- [53] S. Brieden, H. Gil-Marín, and L. Verde, *Model-independent versus model-dependent interpretation of the SDSS-III BOSS power spectrum: Bridging the divide*, *Phys. Rev. D* **104** (2021), no. 12 L121301, [[arXiv:2106.11931](#)].

- [54] S. Brieden, H. Gil-Marín, and L. Verde, *Model-agnostic interpretation of 10 billion years of cosmic evolution traced by BOSS and eBOSS data*, *JCAP* **08** (2022), no. 08 024, [[arXiv:2204.11868](#)].
- [55] M. M. Ivanov, M. Simonović, and M. Zaldarriaga, *Cosmological Parameters from the BOSS Galaxy Power Spectrum*, *JCAP* **05** (2020) 042, [[arXiv:1909.05277](#)].
- [56] G. D’Amico, J. Gleyzes, N. Kokron, K. Markovic, L. Senatore, P. Zhang, F. Beutler, and H. Gil-Marín, *The Cosmological Analysis of the SDSS/BOSS data from the Effective Field Theory of Large-Scale Structure*, *JCAP* **05** (2020) 005, [[arXiv:1909.05271](#)].
- [57] O. H. E. Philcox, M. M. Ivanov, M. Simonović, and M. Zaldarriaga, *Combining Full-Shape and BAO Analyses of Galaxy Power Spectra: A 1.6% CMB-independent constraint on H_0* , *JCAP* **05** (2020) 032, [[arXiv:2002.04035](#)].
- [58] A. Chudaykin, M. M. Ivanov, O. H. E. Philcox, and M. Simonović, *Nonlinear perturbation theory extension of the Boltzmann code CLASS*, *Phys. Rev. D* **102** (2020), no. 6 063533, [[arXiv:2004.10607](#)].
- [59] D. Wadekar, M. M. Ivanov, and R. Scoccimarro, *Cosmological constraints from BOSS with analytic covariance matrices*, *Phys. Rev. D* **102** (2020) 123521, [[arXiv:2009.00622](#)].
- [60] Y. Kobayashi, T. Nishimichi, M. Takada, and H. Miyatake, *Full-shape cosmology analysis of the SDSS-III BOSS galaxy power spectrum using an emulator-based halo model: A 5% determination of σ_8* , *Phys. Rev. D* **105** (2022), no. 8 083517, [[arXiv:2110.06969](#)].
- [61] S.-F. Chen, Z. Vlah, and M. White, *A new analysis of galaxy 2-point functions in the BOSS survey, including full-shape information and post-reconstruction BAO*, *JCAP* **02** (2022), no. 02 008, [[arXiv:2110.05530](#)].
- [62] T. L. Smith, V. Poulin, and T. Simon, *Assessing the robustness of sound horizon-free determinations of the Hubble constant*, [[arXiv:2208.12992](#)].
- [63] J. E. Bautista et al., *The Completed SDSS-IV extended Baryon Oscillation Spectroscopic Survey: measurement of the BAO and growth rate of structure of the luminous red galaxy sample from the anisotropic correlation function between redshifts 0.6 and 1*, *Mon. Not. Roy. Astron. Soc.* **500** (2020), no. 1 736–762, [[arXiv:2007.08993](#)].
- [64] H. Gil-Marín et al., *The Completed SDSS-IV extended Baryon Oscillation Spectroscopic Survey: measurement of the BAO and growth rate of structure of the luminous red galaxy sample from the anisotropic power spectrum between redshifts 0.6 and 1.0*, *Mon. Not. Roy. Astron. Soc.* **498** (2020), no. 2 2492–2531, [[arXiv:2007.08994](#)].
- [65] R. Neveux et al., *The completed SDSS-IV extended Baryon Oscillation Spectroscopic Survey: BAO and RSD measurements from the anisotropic power spectrum of the quasar sample between redshift 0.8 and 2.2*, *Mon. Not. Roy. Astron. Soc.* **499** (2020), no. 1 210–229, [[arXiv:2007.08999](#)].
- [66] J. Hou et al., *The Completed SDSS-IV extended Baryon Oscillation Spectroscopic Survey: BAO and RSD measurements from anisotropic clustering analysis of the Quasar Sample in configuration space between redshift 0.8 and 2.2*, *Mon. Not. Roy. Astron. Soc.* **500** (2020), no. 1 1201–1221, [[arXiv:2007.08998](#)].
- [67] **BOSS** Collaboration, S. Alam et al., *The clustering of galaxies in the completed SDSS-III Baryon Oscillation Spectroscopic Survey: cosmological analysis of the DR12 galaxy sample*, *Mon. Not. Roy. Astron. Soc.* **470** (2017), no. 3 2617–2652, [[arXiv:1607.03155](#)].

- [68] T.-H. Yeh, J. Shelton, K. A. Olive, and B. D. Fields, *Probing Physics Beyond the Standard Model: Limits from BBN and the CMB Independently and Combined*, [arXiv:2207.13133](#).
- [69] H. du Mas des Bourboux et al., *The Completed SDSS-IV Extended Baryon Oscillation Spectroscopic Survey: Baryon Acoustic Oscillations with Ly α Forests*, *Astrophys. J.* **901** (2020), no. 2 153, [[arXiv:2007.08995](#)].
- [70] O. Seto and Y. Toda, *Big Bang Nucleosynthesis constraints on varying electron mass solution to the Hubble tension*, [arXiv:2206.13209](#).

A Supplemental data

In Table 1 we summarize all the resulting constraints in H_0 and Ω_m as shown in the corresponding triangle plots in section Section 3.

Run name	H_0 [km/s/Mpc]	Ω_m
ACDM model		
BAO+BBN	$67.64^{+0.94}_{-1.03}$	$0.293^{+0.015}_{-0.016}$
BAO+BBN+SF+RSD	$68.29^{+0.68}_{-0.69}$	$0.3002^{+0.0060}_{-0.0063}$
BAO(DR12)+BBN(noLUNA)	$68.36^{+1.13}_{-1.25}$	$0.302^{+0.018}_{-0.020}$
BAO+BBN(noLUNA)	$67.90^{+0.92}_{-1.03}$	$0.294^{+0.015}_{-0.016}$
BAO(DR12)+BBN	$68.14^{+1.13}_{-1.24}$	$0.302^{+0.017}_{-0.020}$
BAO(QSO)+BBN	$64.51^{+2.40}_{-2.69}$	$0.347^{+0.049}_{-0.087}$
BAO(LRG)+BBN	$71.18^{+2.27}_{-2.41}$	$0.349^{+0.037}_{-0.035}$
BAO(QSO+LRG)+BBN	$67.88^{+1.10}_{-1.46}$	$0.299^{+0.018}_{-0.025}$
BAO(QSO+Ly α)+BBN	$66.15^{+2.22}_{-2.24}$	$0.302^{+0.035}_{-0.041}$
BAO(DR12 QSO+LRG)+BBN	$72.62^{+2.75}_{-3.56}$	$0.375^{+0.043}_{-0.052}$
BAO+BBN+RSD	$67.66^{+0.90}_{-0.98}$	$0.29^{+0.015}_{-0.016}$
BAO+BBN+SF	$68.30^{+0.66}_{-0.69}$	$0.3023^{+0.0061}_{-0.0063}$
BAO+BBN+SF+RSD (no n_s prior)	$67.70^{+0.91}_{-0.93}$	$0.288^{+0.014}_{-0.013}$
BAO+BBN+RSD (+ A_s prior)	67.88 ± 0.96	$0.293^{+0.017}_{-0.013}$
BAO+BBN+SF+RSD (+ A_s+n_s prior)	$68.25^{+0.88}_{-0.89}$	$0.299^{+0.013}_{-0.014}$
BAO+BBN+SF+RSD (+ A_s prior)	68.47 ± 0.68	0.3001 ± 0.0062
BAO+BBN+ θ_s	$68.16^{+0.48}_{-0.49}$	$0.3022^{+0.0062}_{-0.0064}$
BAO+BBN+SF+RSD+ θ_s	68.30 ± 0.45	$0.3001^{+0.0055}_{-0.0060}$
BAO+BBN+Pantheon	$67.75^{+0.70}_{-0.84}$	$0.296^{+0.011}_{-0.010}$
BAO+BBN+PantheonPLUS	$68.29^{+0.86}_{-0.97}$	$0.311^{+0.011}_{-0.012}$
BAO+BBN+SF+RSD+Pantheon	$68.34^{+0.66}_{-0.65}$	$0.3001^{+0.0057}_{-0.0062}$
BAO+BBN+SF+RSD+PantheonPLUS	$68.20^{+0.67}_{-0.69}$	$0.3036^{+0.0055}_{-0.0062}$
BAO+BBN+CC	$68.12^{+0.90}_{-0.88}$	0.302 ± 0.014
BAO+BBN+SF+RSD+CC	$68.19^{+0.69}_{-0.68}$	$0.3002^{+0.0061}_{-0.0064}$
BAO+BBN+PantheonPLUS+CC	$68.28^{+0.73}_{-0.81}$	$0.311^{+0.011}_{-0.011}$
BAO+BBN+SF+RSD+PantheonPLUS+CC	$68.20^{+0.67}_{-0.68}$	$0.3042^{+0.0058}_{-0.0060}$
N_{eff} ACDM model		
BAO w/ N_{eff}	—	0.293 ± 0.015
BAO+BBN w/ N_{eff}	$66.81^{+1.95}_{-1.93}$	$0.294^{+0.016}_{-0.013}$
BAO+SF w/ N_{eff}	$73.12^{+8.31}_{-6.48}$	$0.288^{+0.009}_{-0.013}$
BAO+BBN+SF w/ N_{eff}	$67.89^{+1.68}_{-1.81}$	0.3009 ± 0.0070
m_e ACDM model		
BAO w/ m_e	—	0.291 ± 0.014
BAO+SF+RSD w/ m_e	$70.82^{+2.81}_{-2.09}$	$0.286^{+0.011}_{-0.016}$
BBN w/ m_e	—	—
BAO+BBN w/ m_e	$66.67^{+1.47}_{-1.83}$	$0.298^{+0.014}_{-0.011}$
BAO+BBN+SF+RSD w/ m_e	$68.21^{+1.12}_{-1.18}$	$0.3009^{+0.0079}_{-0.0080}$

Table 1. Mean and 1σ uncertainty for H_0 and Ω_m for all runs, labeled according to the shorthand notation introduced in Section 2.2 and used in Section 3.